Anharmonicity of graphite from UV Raman spectroscopy to 2700 K

G. Montagnac[a,*], R. Caracas[a], E. Bobocioiu[a], F. Vittoz[b], B.Reynard[a]

[a] *Laboratoire de géologie de Lyon, Ens de Lyon, CNRS UMR5276. 46 allée d'Italie - BP 7000 - 69342 Lyon Cedex 07*
[b] *Laboratoire de physique, Ens de Lyon. 46 allée d'Italie - BP 7000 - 69342 Lyon Cedex 07*

Abstract

First-order Raman spectra of pyrolytic graphite (PG) and highly oriented pyrolytic graphite (HOPG) were recorded *in situ* up to 2670 K and 2491 K, respectively, using a development of wire-loop heating cell technique attached to a UV-Raman spectrometer (244 nm). Raman shift of the E_{2g} in-plane stretching mode of graphite (G band) is used to discuss the anharmonicity by a comparison with calculations in the density-functional theory (DFT). High temperature Raman shifts are well described by anharmonic DFT calculations [1] up to 900 K. Anharmonicity is also determined from the temperature dependence of the Raman linewidth. The quartic term of phonon-phonon scattering process dominates at high temperature with respect to electron-phonon coupling that causes a slight decrease of linewidth with increasing temperature below 1000 K. The G band position is determined with a good reproducibility to 2700 K and can be used as a thermometer for *in situ* studies. Deep UV-Raman proves a viable solution for expanding significantly the temperature range for studying *in situ* vibrational properties of condensed matter, and particularly the monitoring of carbon-based material processing.

1. Introduction

Graphite is the stable allotrope of carbon formed by the stacking of covalent sp^2 layers (the so-called graphene monolayers). It has a vast number of technological applications and is a common mineral in rocks where its Raman spectroscopic features are used to retrieve its formation temperature [2]. In spite of the fundamental interest of this elemental compound, little data exist on the vibrational spectrum of graphite at high temperature [3, 4, 5]. Graphite has a high temperature melting point (> 4000 K [6]), and vaporizes quickly in the 2500-3000 K range at ambient pressure but its vibrational properties are unknown above 900 K. We studied graphite up to 2700 K using developments of a high-temperature cell and UV Raman spectrometry.

Graphite has a simple first-order Raman spectrum and provides a test material for performing *in situ* Raman spectroscopic studies at very high temperatures corresponding to the conditions of elaboration or thermal treatment of many refractory materials. The high temperature limit of Raman spectroscopy is fixed by thermal emission of sample and furnace [7, 8]. According to Planck's equation, the light emitted by a black-body above 1000 K produces an intense background on Raman spectra collected in the visible range. In practice, the Raman signal of a sample heated to about 2000 K is completely hidden whatever its emissivity when excitation in the visible range is used [7, 8, 9]. In order to decrease the effect of thermal emission on Raman measurements, pulsed laser (532 nm) and an optical gating system was used [10, 11] that allowed recording Raman spectra up to 2300 K on hexagonal boron nitride. An alternative to decreasing the photoemission background at higher temperatures is to shift the Raman measurements in UV domain. At 244 nm (5.08 eV), the radiance of a black-body heated to 2600 K is similar to that at 1500 K at 514 nm (2.41 eV) as shown on figure 1. Thus UV Raman spectroscopy is expected to allow analyzing samples *in situ* under very high temperature. This basic idea [12] was tested using a UV argon-ion laser radiation (363.8 nm) on zirconia ceramics up to 1800 K and hafnia ceramics up to 2085 K [13, 14]. Zouboulis et al. [15] performed measurements at even lower wavelength with a quadrupled YAG:Nd^{3+} laser (266 nm) with sapphire as sample up to 1700 K. In these studies the thermal emission was rejected efficiently but the maximum temperature of Raman measurements was not significantly increased with respect to classical Raman spectroscopy using 488 nm visible wavelength on feldspars melts [8] up to 2000 K and on SiO_2 [7, 9] (Fig. 1).

In this work, we present Raman spectra of pyrolytic graphite (PG) and highly oriented pyrolytic graphite (HOPG) up to 2700 K using 244 nm excitation wavelength. Surprisingly, those allotropic forms of carbon have never been studied with Raman spectroscopy at very high temper-

*Corresponding author: Gilles Montagnac
Tel: +33 4 72 72 84 07
Fax: +33 4 72 72 86 77
Email address: gilles.montagnac@ens-lyon.fr (G. Montagnac)

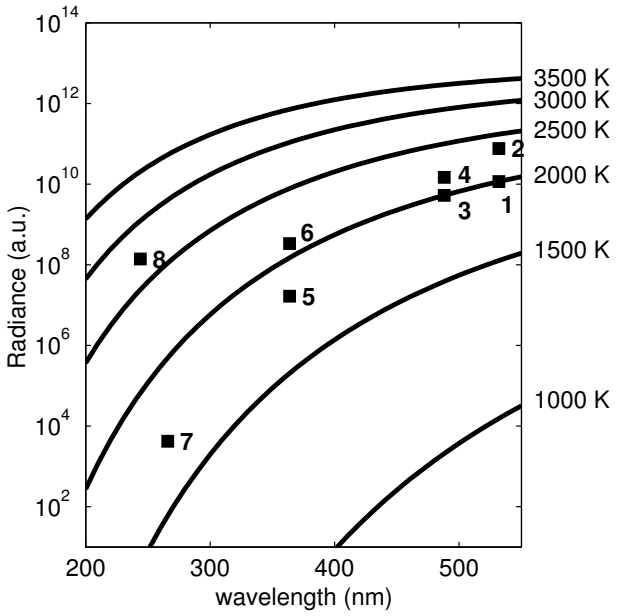

Figure 1: Spectral radiance of the black-body radiation emitted for several temperatures (from 1000 K to 3500 K) as a function of wavelength according to the Planck's law. Filled squares indicate experimental conditions of *in situ* Raman spectroscopic studies at high temperature: **1** Simon et al. [11] **2** Exarhos and Schaaf [10] **3** McMillan et al. [7] and Daniel et al. [8] **4** Kalampounias et al. [9] **5** Yashima et al. [13] **6** Fujimori et al. [14] **7** Zouboulis et al. [15] **8** This work.

ature. Tan et al. [4] reported anomalous Raman phenomenon related to the wavelength excitation on HOPG and the temperature effect of the laser power on the spectra up to 647 K. Temperature evolution of infrared- and Raman-active phonons in graphite was measured in the range 293-523 K by Giura et al. [5]. Here, we have followed the 244 nm first-order Raman spectrum of PG and HOPG confined in a new wire-loop heating stage coupled to the Raman apparatus. Comparison of the predicted and measured shifts and linewidth is used to discuss anharmonicity of the G mode of graphite.

2. Methodology

2.1. The high temperature cell

A prototype was designed to heat samples up to 3200 K and perform UV Raman measurements. It was inspired from a wire-loop heating stage design [16], where the furnace is a filament heated by Joule effect. Alloy of $Pt_{90}Ir_{10}$ can be used as a wire up to 2000 K (near its melting point). Higher temperatures are achieved with Ir or Re wire [17]. Re has better mechanical properties and a higher melting point than Ir (3450 *vs* 2700 K respectively). A 50 mm length, 0.5 mm of diameter wire is pressed in its middle down to a 250 μm thickness over a length of 2 mm. The sample is as rectangular piece of 300 - 400 μm, packed in a hole of 400 μm drilled in the flat surface shaped in the middle of the rod. Excepted for Pt, PGE (platinum

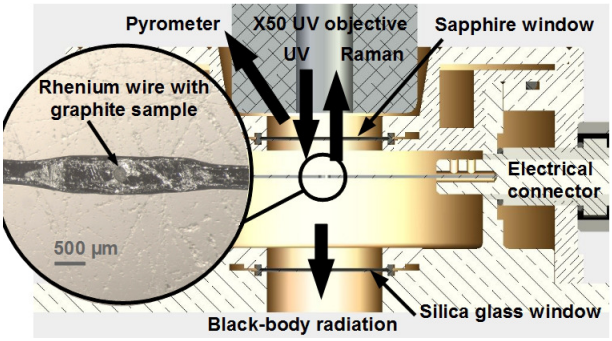

Figure 2: Sectional view of the wire-loop heating stage. The zoom is a picture of the heating rhenium wire with the sample confined in a 400 μm of diameter hole. Pyrometric and UV Raman measurements are performed alternatively through the sapphire window. Black-body radiation can be recorded simultaneously in the 400-1200 nm range through the silica glass window at the bottom of the cell.

group elements) rods are very hard and difficult to shape. Re wires are annealed at high temperature ($\approx$ 2000 K) prior to flattening. Since electrical conductivity is affected by cycling at high temperature, the relationship between temperature and electrical power input to the wire must be regularly recalibrated [18]. As an alternative of this furnace, we also used a 50 mm length PG rod with a diameter of 1 mm. Electrical connectors at the extremities of the wire are plugged to a 10 V, 75 A power supply from Nemic Lambda™. The wire is fixed to a connector and can slide in the other while keeping electric contact to allow for dilatation during heating. The heating stage can reach 2200 K with PG wire and 3200 K with Re wire. Different diameters from 0.5 to 2 mm of both material have been tested for a fixed wire length. The dimensions used are a compromise between fragility and electrical resistance supported by the supply to reach the maximum temperature. The cell walls are cooled by a water flow in order to maintain the isolated electric connectors crossing the walls at a reasonable temperature. A reducing mixture of argon and 2.4 % hydrogen (Arcal™ 10) is flown in the cell at the rate of 1 l/min to avoid oxidation and combustion of the heated elements. Spectroscopic and pyrometric measurements are performed through a UV quality sapphire cleaved perpendicular to the c axis. Dimensions of this window, 0.45 mm thick and 25 mm in diameter, allow alternating quickly from temperature measurement with a pyrometer (placed at an angle of 30°) to Raman measurement with a vertical microscope entrance to the spectrometer. Optical transmittance of the sapphire window is around 80 % at 244 nm wavelength. Finally, visible-range of the black-body radiation was collected through a thin silica glass window placed at the bottom of the cell (Fig. 2).

2.2. Temperature measurement

The use of thermocouples is impossible in the wire-loop setup, and external calibrations are of limited use because of oxidation or aging of the wire [18]. Thus non-contact methods of temperature measurements have to be used.

The intensity ratio of the Stokes and Anti-Stokes lines cannot be used because it is impossible to record the anti-Stokes region with the edge filter used in our UV Raman apparatus. Variation of the emissivity of the sample and the importance of temperature gradients between furnace and sample lead us to use spectrometric methods to determine the temperature. A Keller MSR™ two-colour pyrometer with a telephoto lens (100 mm working distance) was focused on the sample. Its field of view gives a target diameter of ≈ 400 μm. It operates in the range 1123 K-3273 K. The measurements were verified for two melting points, Ag and Mg_2SiO_4 forsterite, at 1235 K and 2163 K respectively with an accuracy of ± 5 degrees. For each temperature measurement performed with the pyrometer, thermal emission was recorded with a visible-range spectrometer from 400 nm to 1200 nm through the silica window at the bottom of the cell. The system response was calibrated with the sample spectrum at 1235 K (the melting point of Ag). Spectra have been treated with the program "Shades of Gray" [19]. Parts of the emission spectra recorded from 400 to 1200 nm, are fitted with three methods, according to the Planck's distribution, the Wien's approximation and a sliding two colour pyrometry. We found a good agreement between pyrometric measurement and fits to emission spectra (Fig. 3) with an average deviation of less than 3% whatever the method used. From room temperature to 873 K, UV Raman measurements have also been performed in a Linkam™ heating cell where temperature is measured by a thermocouple. We substituted the window of this heating cell by a UV quality sapphire window. Raman measurement at 514 and 244 nm have been compared. Shifts of Raman peaks with temperature is independent on wavelength, demonstrating the absence of significant heating effects of the lasers.

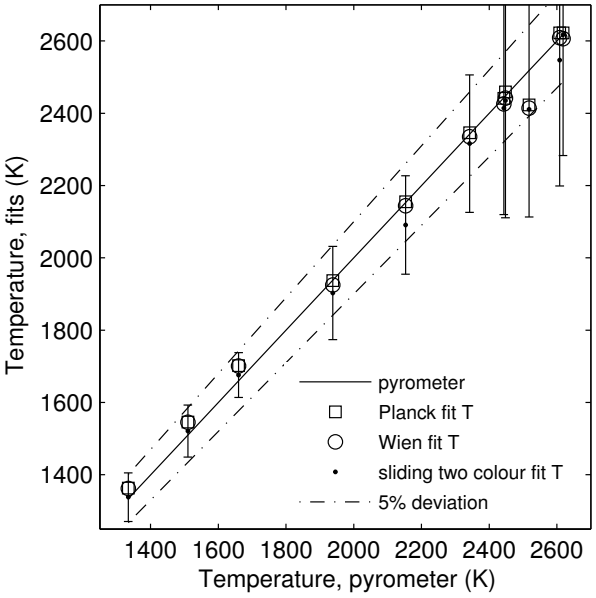

Figure 3: Comparison of temperature fits of thermal emission spectra with pyrometric measurements. The solid line is the 1:1 correlation. The errors for Planck and Wien fits are within the symbol size (□ and ◯). The dot dashed lines indicate ±5% deviation from pyrometry temperature.

2.3. UV and visible Raman apparatus

We used two Horiba Jobin-Yvon LabRam HR800™ Raman micro-spectrometers. Below 1200 K, measurements have been performed with both 514.5 nm and 244 nm excitation wavelength. For higher temperatures, only the 244 nm wavelength was used. The edge filter used in the UV device cuts the signal below 300 cm^{-1}, precluding the study of the lowest frequency Raman mode of graphite. The UV light source is composed of an argon ion laser tuned blue (488 nm) and frequency doubled by a BBO crystal in an external cavity (Spectra Physics Wavetrain™).

With UV excitation, the damage of the sample can occur, especially when it contains organic molecules [20, 21]. The power of the laser beam was kept below 800 μW on PG or HOPG and exposure time below 240 seconds for longest acquisitions at high temperature. In these conditions, no transformation of the Raman spectra was noted during laser exposition of the sample. This is not the case for laser power above 1 mW and/or exposure time longer than 300 seconds. Damage was visible on the sample surface and the G band decreased in intensity, increased in width, and became asymmetric. This illustrates a threshold effect of the laser power and time exposure.

Given that 244 nm is not a usual wavelength in microscopy, we used a specially designed Mitutoyo™ objective with 11 mm long working distance and 80% transmission both at 244 nm and in the visible domain. The laser spot focused on the sample is about 3μm in diameter. Thus the Raman signal is only collected from the sample without contribution from the furnace. Above 1200 K, the intense visible light emitted by the sample and the wire penetrates through the slit into the spectrometer. Even if this light is not diffracted by the grating and not focused, it generates background with a step shape on the spectrum. A UV bandpass interference filter centered on 253 nm was used to reject the visible radiation. With 10 nm of full width at half maximum (FWHM), the transmission of this filter can be considered as constant ($\approx 15\%$) all along the range of the first-order Raman band shift of graphite with temperature.

2.4. First-principles phonon calculations

We computed the position of the Raman and infrared peaks of graphite using first-principles calculations based on the density-functional (DFT) [22] and density-functional perturbation theories (DFPT) [23, 24, 25] in the ABINIT implementation [26, 27] with plane-waves and norm-conserving pseudo-potentials [28, 29]. We employed a kinetic-energy cut-off of 40 Ha (1 Ha = 27.2116 eV) and a 8x8x4 grid of high-symmetry special k points [30].

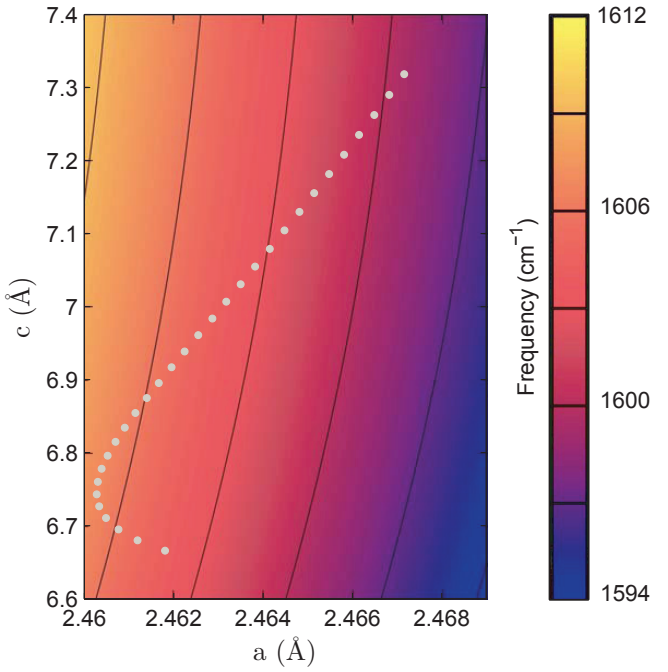

Figure 4: Contour plot of the frequency of the E_{2g} Raman active mode as a function of lattice parameters. All calculations are static; lattice parameters range cover experimental values up to 3000 K (grey dots).

While our grid of k points is rather smaller than others used in previous studies (e.g. in Mounet and Marzari [31], where the thermodynamic parameters are computed from the lattice dynamical calculations and the quasi-harmonic approximation), our phonon frequencies are in good agreement with experimental measurements. In order to compute the Raman tensors, a fixed electronic occupation of 2 electrons/band was used. The grid of k points was shifted so that the gap is always non-zero in the calculations.

We performed the calculations at several unit cell parameters a (in-plane) and c (out of plane) such as to cover all the possible values spanned by the increase in temperature (Fig. 4). All calculations are static, *i.e.* at absolute null temperature. The intensity of the first-order Raman peaks is obtained computing the Raman tensors in DFPT [32, 33]; the procedure is described in detail elsewhere [34].

3. Results and discussion

3.1. Raman spectra of PG and HOPG

According to group theory, the 12 phonon modes in the Brillouin zone center decompose as $2A_{2u} \oplus 2B_{2g} \oplus 2E_{1u} \oplus 2E_{2g}$. The acoustic modes are A_{2u} and E_{1u}. Only the E_{2g} modes are Raman active. The results of the phonon calculations performed at static conditions and experimental unit cell volume are summarized in Table 1. The first theoretical E_{2g} Raman active mode is at 42 cm^{-1} and out of the present experimental range, the second E_{2g} mode

Label	TO frequency (cm^{-1})	LO frequency (cm^{-1})	Raman intensity
E_{2g}	42	42	40%
B_{2g}	89	89	
B_{2g}	902	902	
A_{2u}	906	906	
E_{2g}	1603	1603	100%
E_{1u}	1616	1616	

Table 1: Computed phonon frequencies

is at 1603 cm^{-1}. The measured first order Raman spectrum of well ordered defect free samples shows a single line at 1582 cm^{-1} named G band and related to an in-plane phonon with symmetry E_{2g} [35]. The difference in peak position between experiment and theory is mainly due to the harmonic approximation that neglects high-order terms in the perturbation expansion of the lattice energy in DFPT [23, 24, 25].

The graphite furnace used in the heating cell is a pyrolytic graphite (PG) rod. It is the result of compacted isotropic ultra-fine grained pure PG. The 514.5 nm Raman spectra present defect bands D and D' respectively at 1355 cm^{-1} and 1620 cm^{-1}. The frequencies of these bands change with changing laser wavelength [36] and I(D)/I(G) intensity ratio is dispersive [37, 38]. D and D' bands are not observed in the 244 nm UV-Raman spectrum. In contrast the G band corresponding to sp^2 bond stretching is strong.

The highly oriented pyrolytic graphite (HOPG) is grown with an almost perfect alignment perpendicular to the carbon plane. Along the in-plane directions, the crystallites are small and randomly oriented. D and D' bands are observed in the Raman spectrum of HOPG edge planes excited with 514.5 nm excitation [39], but not with 244 nm excitation.

Representative first-order Raman spectra are plotted on figure 5 for different temperatures with visible and UV excitation. This illustrates the advantage of UV Raman scattering with respect to the visible range excitation. The absence of background on spectra up to 2300 K allows easily following the G band. The peak position and shape was fitted with a Lorentzian shape. A linear background correction was applied up to 2300 K. Above this temperature, we subtracted to the signal the thermal emission spectrum collected on the sample without laser excitation [8].

3.2. Anharmonicity of the G band

The Raman shift of G band of PG and HOPG has been recorded as a function of temperature from 295 K to 2670 K and 2490 K, respectively (Fig. 6). Kagi et al. [3] have reported on PG a down-shift of 12 cm^{-1} when temperature increased from 400 K to 890 K, and Tan et al. [4] have reported a Raman shift of the G band of HOPG of 1578 cm^{-1} at 648 K, both consistent with our data. On HOPG, we observe a phonon frequency shift similar to

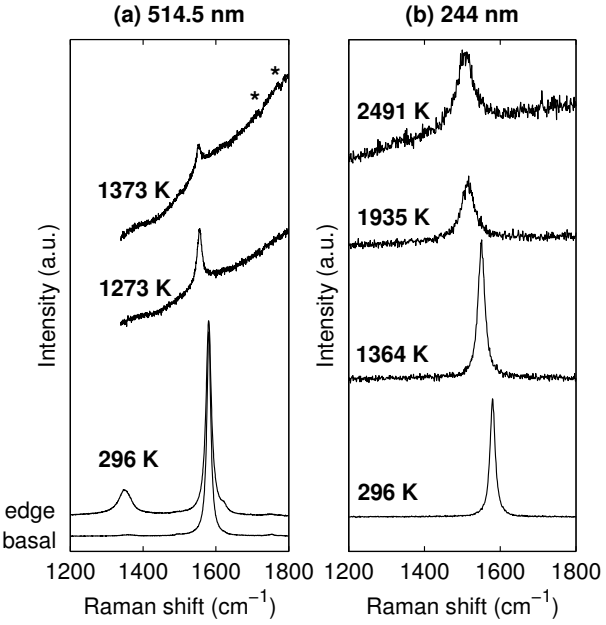

Figure 5: Representative first-order Raman spectra (uncorrected) of HOPG illustrating the advantage of the UV Raman scattering for extending the temperature range of measurements to 2500 K. Basal and edge orientations present different Raman spectra only with visible excitation. Defects on CCD detector are visible in spectra with strong background intensity (∗).

PG up to 1250 K. Above this temperature, there is a slight down-shift of PG with respect to HOPG in the range 1500-2500 K. This may be attributed to shorter crystal planar domain size in PG than HOPG. Our estimation of the temperature dependence of the G band is -0.02 cm^{-1}/K for temperatures below 800 K, in the average of the values encountered for different carbonaceous materials [40].

The frequency change with temperature at constant pressure arises from contributions of a quasiharmonic term (noted qh) associated with volume expansion with temperature, and from a volume independent or intrinsic anharmonic effect:

$$\left(\frac{\partial \ln \nu}{\partial T}\right)_P = \left(\frac{\partial \ln \nu}{\partial T}\right)_V + \left(\frac{\partial \ln \nu}{\partial \ln V}\right)_T \left(\frac{\partial \ln V}{\partial T}\right)_P \quad (1)$$

$$= a - (\alpha \cdot \gamma)_{qh}. \quad (2)$$

where $\gamma = -(\partial \ln \nu / \partial \ln V)_T$ is the Grüneisen parameter, $\alpha = (\partial \ln V / \partial T)_P$ the thermal expansion and $a = (\partial \ln \nu / \partial T)_V$ the intrinsic anharmonic parameter.

The quasi-harmonic shift of Raman mode E_{2g} assigned to G band was obtained from the present first-principles calculations. The E_{2g} mode is an in-plane stretching mode whose frequency depends both on absolute volume but also on variations of the c/a lattice parameter ratio. Frequencies calculated from a set of a and c values covering the whole range of measured values up to 3000 K by Morgan [41] were fitted with second-order polynomial expressions for interpolation (Fig. 4). Interpolated values were calculated for the experimental volumes [41] to obtain the quasiharmonic temperature variation (Fig. 6). The theoretical qh. values are compared with extrapolation of the high pressure measurements of vibrational frequency and volume of graphite [42] to the high temperature cell parameters. Because of the large anisotropy of the graphite crystal [43], it is useful to define the Grüneisen parameter γ of the E_{2g} mode as a function of the lattice parameter a instead of volume:

$$\frac{\nu(P)}{\nu_0} = \left(\frac{\mathrm{a}(P)}{\mathrm{a}_0}\right)_T^{-3\gamma} \quad (3)$$

yielding a value of $\overline{\gamma} = 1.06$ [42]. Both the extrapolation of the high-pressure data and the theoretical qh. values give slightly positive quasi-harmonic shifts up to 1000 K, that become negative at higher temperatures to reach about -10 cm^{-1} at 2700 K. This evolution matches the behavior of the a parameter that contracts to 1000 K before expanding at higher temperatures. The large difference between theoretical qh. and measured values of Raman shift is due to intrinsic anharmonicity of this vibrational mode at high temperature. The difference is used to calculate the intrinsic anharmonic parameter assumed constant over the whole temperature range [44]:

$$a = \left(\frac{\Delta \ln \nu_{th}}{\Delta T}\right)_V \quad (4)$$

A value of $a = -1.84 \cdot 10^{-5}$ K^{-1} is obtained.

Recent *ab initio* models of graphite and graphene by Bonini et al. [1] include a quasiharmonic contribution induced by the change of the lattice thermal expansion and an anharmonic contribution due to phonon-phonon interaction at fixed lattice spacing that explains the strong decrease of the line-shift with increasing temperature. This model accurately predicted experimental Raman shifts measured up to 700 K [5].

In order to compare our measurements at higher temperatures with this anharmonic first principles calculations, we used analytic expression from Klemens [45] and Balkanski et al. [46] to fit the data:

$$\begin{aligned}\nu(T) = \nu_0 + A\left(1 + 2f_1\left(\frac{x}{2}\right)\right) \\ + B\left(1 + 3f_1\left(\frac{x}{3}\right) + 3f_1^2\left(\frac{x}{3}\right)\right)\end{aligned} \quad (5)$$

It describes the effects of high-order phonon-phonon interactions on Raman line-shift. In this equation, $x = hc\nu_0/k_BT$ and $f_1(x) = 1/(\exp(x)-1)$ terms describe phonon population at thermal equilibrium in Bose-Einstein distribution. ν_0, A and B are constants.

Theoretical data [1] are plotted in figure 6 and vertically shifted to be compared to experimental data at $T = 295$ K. They are consistent with our measurements up to 900 K. Theoretical data have been extrapolated assuming $B = 0$ in equation (5). This implies that terms

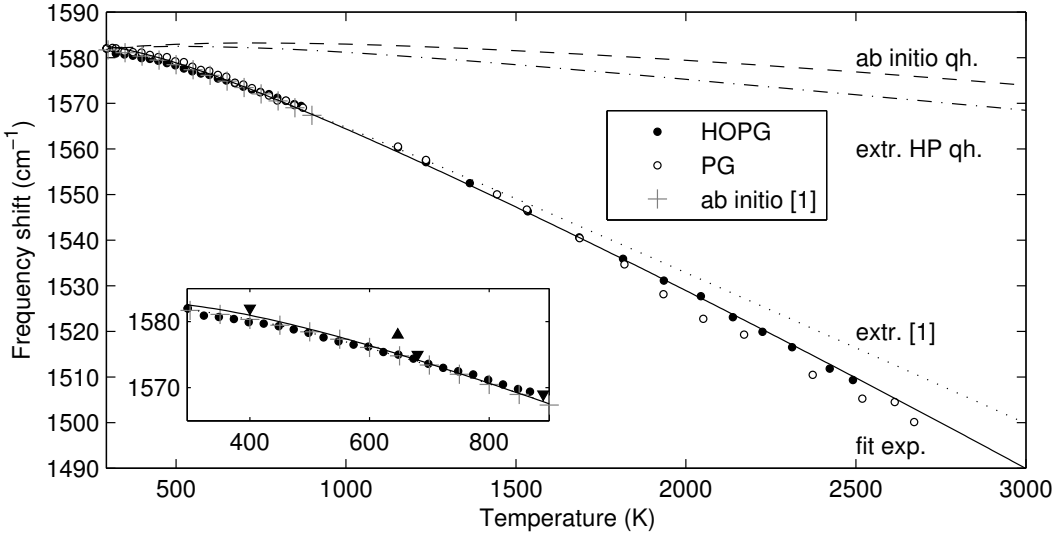

Figure 6: Frequency shift of the G band of PG (open circles) and HOPG (black filled circles) collected with 244 nm excitation wavelength. Data from Kagi et al. [3] (▼) and Tan et al. [4] (▲) are shown. Dashed line: theoretical quasi-harmonic shift; dot-dashed line: extrapolation of high pressure data from Hanfland et al. [42]; doted line: high-temperature extrapolation of theoretical data (+) from Bonini et al. [1] using equation (5). The black solid line is the fit of HOPG measurements using equation (5) (parameters of the fit are discussed in the text).

proportional to $\hbar^2$ in the anharmonic vibrational Hamiltonian [46] are ignored because they are assumed to be of a lower magnitude. This results in a linear behavior of the line-shift with temperature above 1000 K that slightly underestimates the temperature dependence of experimental Raman shifts at very high temperature. Constants determined from this fit are $\nu_0 = 1602$ cm^{-1} and $A = -19.37$ cm^{-1}. In order to better describe the experimental data at high temperature, we added a quartic contribution by fitting B in equation (5) with ν_0 and A values determined above, yielding $B = -0.237$ cm^{-1}. This contribution is about two orders of magnitude lower than other anharmonic contributions, but has a measurable influence on line-shift at very high temperature.

The evolution of the linewidth with temperature also reflects the anharmonic behavior of graphite layers (Fig. 7). For HOPG the linewidth increases with a strong curvature above 1000 K that is typical of phonon-phonon interactions involving decay processes with production of two and three phonons [45, 46]. In addition to the phonon-phonon contributions, phonon-electron coupling results in negative temperature dependence of linewidth to 900 K in graphite [1, 47, 48]. Assuming both coupling effects and decay to 2 and 3 phonons with energies of one half and one third of the energy of the initial mode, the linewidth is expressed as:

$$\begin{aligned}\Gamma(T) = \Gamma_0 &+ C\left(1 + 2f_1\left(\frac{x}{2}\right)\right) \\ &+ D\left(1 + 3f_1\left(\frac{x}{3}\right) + 3f_1^2\left(\frac{x}{3}\right)\right) \\ &+ \Gamma^{\text{e-ph}}(0)\left(f_2\left(-\frac{x}{2}\right) - f_2\left(\frac{x}{2}\right)\right)\end{aligned} \tag{6}$$

where $f_2(x) = 1/(\exp(x) + 1)$. Linewidth at 0 K, $\Gamma^{\text{e-ph}}(0)$, is 9.8 cm^{-1} for the electron-phonon coupling [47]. Γ_0, C and D constants were fitted to the data, yielding, 3.84 cm^{-1}, 1.31 cm^{-1} and 0.89 cm^{-1}, respectively. The Γ_0 value includes a contribution from the bandpass of the Raman spectrometer. Two regions can be distinguished, one below 1000 K where the electron-phonon coupling compensates the phonon-phonon coupling, with a slightly negative temperature dependence [1], and one above 1000 K a large increase of linewidth with temperature due to a dominant quartic decay contribution.

For PG, the evolution of linewidth is very different from HOPG below 1000 K. A strong increase in linewidth is observed at moderate temperature. We attribute this effect to possible impurities in the industrial PG (99.95 % pure graphite). The convergence of linewidth of the two allotropes above 1000 K may indicate that these impurities are eliminated during high temperature treatment.

We have estimated intensities of the Raman G band from peak areas. They are little or not affected by temperature within uncertainties at high temperature.

3.3. Potential of UV Raman spectroscopy at high temperatures

The present study illustrates the potential of UV-Raman spectroscopy for expanding the temperature range of in situ investigations. Further improvements rely on modifications of the setup. UV Raman measurements are limited above 300 cm^{-1} because of the cutting of the Raman edge filter. The decrease in quantum efficiency of the multichannel CCD detector in the UV domain of wavelength ($\approx 30\%$ of a visible signal) is counterbalanced by the gain of UV Raman scattering cross section. The Raman cross

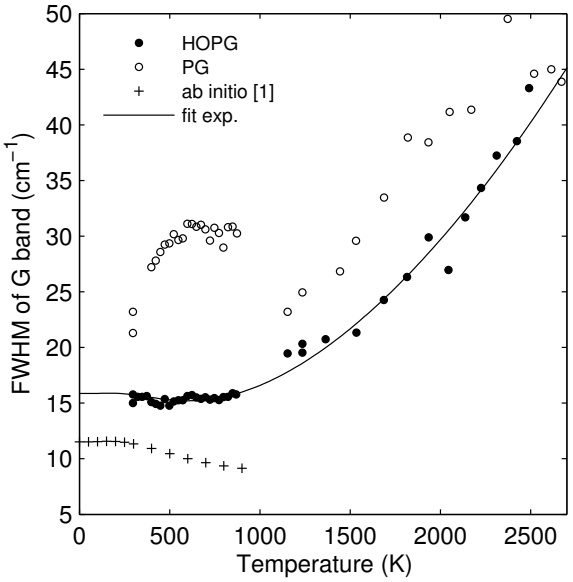

Figure 7: Linewidth (full width at half maximum FWHM) of Raman G band for HOPG (filled circles) and PG (open circles) as a function of temperature. The solid line is a fit to the data according to an anharmonic model (equation (6)). Theoretical data (+) from Bonini et al. [1] are shown.

section σ_{RS} is proportional to the square of the polarizability derivative from the m to n vibrational transition and the fourth power of the scattering frequency has been quantified [49].

UV Raman spectroscopy is effective in reducing the masking effect of thermal emission, even if a UV bandpass interference filter with a 15% transmission has to be added to further eliminate stray visible light. This allowed investigating *in situ* the ultra high temperature domain to at least 2700 K, instead of the 2150 K reached with visible excitation. The temperature limit of the present measurements is due to the rapid sublimation of graphite above 2500 K. We obtained a reproducible calibration of the G band position with temperature from 295 K up to 2700 K for both PG and HOPG. Graphite rods can be used both as an easy-to-shape furnace in the wire-loop design, and as an internal temperature sensor. Analyzed Raman spots on sample and on PG rod must be as close as possible, less than 50 μm, to avoid temperature gradient effects at this scale. An empirical formula is used to describe the temperature dependence of the Raman G mode:

$$\nu_G(T) = \nu_{296K} - \frac{A}{\exp(Bhc\nu_{296K}/kT) - 1} \qquad (7)$$

where $\nu_{296K} = 1582$ cm^{-1} is the Raman shift at 296 K. We have used Eq. (7) to fit our measurements on PG with parameters $A = 67.4$ cm^{-1} and $B = 0.702$ given a root mean square error of 0.84 cm^{-1}. On HOPG parameters $A = 57.85$ cm^{-1} and $B = 0.645$ given a root mean square error of 0.48 cm^{-1}. By inverting Eq (7), the temperature is obtained from the change of Raman shift $\Delta\nu = \nu_{296K} - \nu_G$ according to:

$$T = \frac{Bhc\nu_{296K}}{k\ln(1 + A/\Delta\nu)} \qquad (8)$$

with a precision of $\Delta T = \pm 6$ K in the 95% confidence limit for PG and $\Delta T = \pm 4$ K for HOPG. The accuracy is estimated to be 3% in the range 1500-2500 K from average deviation of the various temperature measurements.

The evolution of frequency and linewidth determined here for graphite provides a basis for monitoring *in situ* high-temperature transformations in the processing of carbonaceous material with Raman spectroscopy.

Acknowledgments

The Raman facility in Lyon is supported by the Institut National des Sciences de l'Univers (INSU). J. P. Perrillat and M. Mezouar for access to "Shade of gray" algorithms developed at the ID27 beamline of ESRF. Calculations have been performed on the JADE machine of CINES under grant DARI stl2816 and on the local resources at PSMN of ENS Lyon. Insightful comments from two anonymous reviewers help to improve the manuscript. M. Lazzeri kindly provided the anharmonic DFT data and useful comments.

References

[1] Bonini, N., Lazzeri, M., Marzari, N., Mauri, F.. Phonon anharmonicities in graphite and graphene. Phys Rev Lett 2007;99:176802.

[2] Beyssac, O., Goff, B., Chopin, C., Rouzaud, J.N.. Raman spectra of carbonaceous material in metasediments: a new geothermometer. Journal of Metamorphic Geology 2002;20(9):859–871.

[3] Kagi, H., Tsuchida, I., Wakatsuki, M., Takahashi, K., Kamimura, N., Iuchi, K., et al. Proper understanding of down-shifted raman spectra of natural graphite: Direct estimation of laser-induced rise in sample temperature. Geochimica et Cosmochimica Acta 1994;58(16):3527 – 3530.

[4] Tan, P.H., Deng, Y.M., Zhao, Q.. Temperature-dependent raman spectra and anomalous raman phenomenon of highly oriented pyrolytic graphite. Phys Rev B 1998;58:5435–5439.

[5] Giura, P., Bonini, N., Creff, G., Brubach, J.B., Roy, P., Lazzeri, M.. Temperature evolution of infrared- and raman-active phonons in graphite. Phys Rev B 2012;86:121404.

[6] Savvatimskiy, A.. Measurements of the melting point of graphite and the properties of liquid carbon (a review for 19632003). Carbon 2005;43(6):1115 – 1142.

[7] McMillan, P., Poe, B., Gillet, P., Reynard, B.. A study of sio2 glass and supercooled liquid to 1950 k via high-temperature raman spectroscopy. Geochimica et Cosmochimica Acta 1994;58(17):3653 – 3664.

[8] Daniel, I., Gillet, P., Poe, B.T., McMillan, P.F.. In-situ high-temperature raman spectroscopic studies of aluminosilicate liquids. Physics and Chemistry of Minerals 1995;22:74–86.

[9] Kalampounias, A.G., Yannopoulos, S.N., Papatheodorou, G.N.. Temperature-induced structural changes in glassy, supercooled, and molten silica from 77 to 2150 K. The Journal of Chemical Physics 2006;124(1):014504.

[10] Exarhos, G.J., Schaaf, J.W.. Raman scattering from boron nitride coatings at high temperatures. Journal of Applied Physics 1991;69(4):2543–2548.

[11] Simon, P., Moulin, B., Buixaderas, E., Raimboux, N., Herault, E., Chazallon, B., et al. High temperatures and raman scattering through pulsed spectroscopy and ccd detection. Journal of Raman Spectroscopy 2003;34(7-8):497–504.

[12] Farrow, R.L., Nagelberg, A.S.. Raman spectroscopy of surface oxides at elevated temperatures. Applied Physics Letters 1980;36(12):945–947.

[13] Yashima, M., Kakihana, M., Shimidzu, R., Fujimori, H., Yoshimura, M.. Ultraviolet 363.8-nm raman spectroscopic system for in situ measurements at high temperatures. Applied Spectroscopy 1997;51(8):1224–1228.

[14] Fujimori, H., Kakihana, M., Ioku, K., Goto, S., Yoshimura, M.. Advantage of anti-stokes raman scattering for high-temperature measurements. Applied Physics Letters 2001;79(7):937–939.

[15] Zouboulis, E., Renusch, D., Grimsditch, M.. Advantages of ultraviolet raman scattering for high temperature investigations. Journal of Applied Physics 1998;72(1):1–3.

[16] Mysen, B.O., Frantz, J.D.. Raman spectroscopy of silicate melts at magmatic temperatures: Na_2O-SiO_2, K_2O-SiO_2 and Li_2O-SiO_2 binary compositions in the temperature range 25-1475 C. Chemical Geology 1992;96(34):321 – 332.

[17] Fiquet, G., Richet, P., Montagnac, G.. High-temperature thermal expansion of lime, periclase, corundum and spinel. Physics and Chemistry of Minerals 1999;27:103–111.

[18] Richet, P., Gillet, P., Pierre, A., Bouhifd, M.A., Daniel, I., Fiquet, G.. Raman spectroscopy, x-ray diffraction, and phase relationship determinations with a versatile heating cell for measurements up to 3600 K (or 2700 K in air). Journal of Applied Physics 1993;74(9):5451–5456.

[19] Benedetti, L.R., Loubeyre, P.. Temperature gradients, wavelength-dependent emissivity, and accuracy of high and very-high temperatures measured in the laser-heated diamond cell. High Pressure Research 2004;24(4):423–445.

[20] Quirico, E., Montagnac, G., Lees, V., McMillan, P.F., Szopa, C., Cernogora, G., et al. New experimental constraints on the composition and structure of tholins. Icarus 2008;198, Issue 1:218–231.

[21] Quirico, E., Montagnac, G., Rouzaud, J.N., Bonal, L., Bourot-Denise, M., Duber, S., et al. Precursor and metamorphic condition effects on raman spectra of poorly ordered carbonaceous matter in chondrites and coals. Earth and Planetary Science Letters 2009;287:185–193.

[22] Kohn, W., Sham, L.J.. Self-consistent equations including exchange and correlation effects. Phys Rev 1965;140:A1133–A1138.

[23] Baroni, S., de Gironcoli, S., Dal Corso, A., Giannozzi, P.. Phonons and related crystal properties from density-functional perturbation theory. Rev Mod Phys 2001;73:515–562.

[24] Gonze, X., Rignanese, G.M., Caracas, R.. First-principles studies of the lattice dynamics of crystals, and related properties. Zeitschrift für Kristallographie 2005;220:458–472.

[25] Caracas, R., Gonze, X.. Thermodynamic Properties of Solids: Experiment and Modeling. Wiley-VCH Verlag, Weinheim; 2010. Lattice dynamics and thermodynamical properties.

[26] Gonze, X., Beuken, J.M., Caracas, R., Detraux, F., Fuchs, M., Rignanese, G.M., et al. First-principles computation of material properties: the abinit software project. Computational Materials Science 2002;25(3):478 – 492.

[27] Gonze, X., Amadon, B., Anglade, P.M., Beuken, J.M., Bottin, F., Boulanger, P., et al. Abinit: First-principles approach to material and nanosystem properties. Computer Physics Communications 2009;180(12):2582 – 2615.

[28] Payne, M.C., Teter, M.P., Allan, D.C., Arias, T.A., Joannopoulos, J.D.. Iterative minimization techniques for *ab initio* total-energy calculations: molecular dynamics and conjugate gradients. Rev Mod Phys 1992;64:1045–1097.

[29] Troullier, N., Martins, J.L.. Efficient pseudopotentials for plane-wave calculations. Phys Rev B 1991;43:1993–2006.

[30] Monkhorst, H.J., Pack, J.D.. Special points for brillouin-zone integrations. Phys Rev B 1976;13:5188–5192.

[31] Mounet, N., Marzari, N.. First-principles determination of the structural, vibrational and thermodynamic properties of diamond, graphite, and derivatives. Phys Rev B 2005;71:205214.

[32] Lazzeri, M., Mauri, F.. First-principles calculation of vibrational raman spectra in large systems: Signature of small rings in crystalline sio$_2$. Phys Rev Lett 2003;90:036401.

[33] Veithen, M., Gonze, X., Ghosez, P.. Nonlinear optical susceptibilities, raman efficiencies, and electro-optic tensors from first-principles density functional perturbation theory. Phys Rev B 2005;71:125107.

[34] Caracas, R., Bobocioiu, E.. The wurm projecta freely available web-based repository of computed physical data for minerals. American Mineralogist 2011;96(2-3):437–443.

[35] Tuinstra, F., Koenig, J.L.. Raman spectrum of graphite. The Journal of Chemical Physics 1970;53(3):1126–1130.

[36] Thomsen, C., Reich, S.. Double resonant raman scattering in graphite. Phys Rev Lett 2000;85:5214–5217.

[37] Vidano, R., Fischbach, D., Willis, L., Loehr, T.. Observation of raman band shifting with excitation wavelength for carbons and graphites. Solid State Communications 1981;39(2):341 – 344.

[38] Pócsik, I., Hundhausen, M., Koós, M., Ley, L.. Origin of the d peak in the raman spectrum of microcrystalline graphite. Journal of Non-Crystalline Solids 1998;227230, Part 2(0):1083 – 1086.

[39] Tan, P., Dimovski, S., Gogotsi, Y.. Raman scattering of nonplanar graphite: arched edges, polyhedral crystals, whiskers and cones. Philosophical Transactions of the Royal Society of London Series A:Mathematical, Physical and Engineering Sciences 2004;362(1824):2289–2310.

[40] Calizo, I., Balandin, A.A., Bao, W., Miao, F., Lau, C.N.. Temperature dependence of the raman spectra of graphene and graphene multilayers. Nano Letters 2007;7(9):2645–2649.

[41] Morgan, W.. Thermal expansion coefficients of graphite crystals. Carbon 1972;10(1):73 – 79.

[42] Hanfland, M., Beister, H., Syassen, K.. Graphite under pressure: Equation of state and first-order raman modes. Phys Rev B 1989;39:12598–12603.

[43] Zallen, R.. Pressure-raman effects and vibrational scaling laws in molecular crystals: S_8 and As_2S_3. Phys Rev B 1974;9:4485–4496.

[44] Gillet, P., Daniel, I., Guyot, F.. Anharmonic properties of Mg_2SiO_4-forsterite measured from the volume dependence of the raman spectrum. European Journal of Mineralogy 1997;9(2):255–262.

[45] Klemens, P.G.. Anharmonic decay of optical phonons. Phys Rev 1966;148:845–848.

[46] Balkanski, M., Wallis, R.F., Haro, E.. Anharmonic effects in light scattering due to optical phonons in silicon. Phys Rev B 1983;28:1928–1934.

[47] Lazzeri, M., Piscanec, S., Mauri, F., Ferrari, A.C., Robertson, J.. Phonon linewidths and electron-phonon coupling in graphite and nanotubes. Phys Rev B 2006;73:155426.

[48] Ferrari, A.C.. Raman spectroscopy of graphene and graphite: Disorder, electron-phonon coupling, doping and nonadiabatic effects. Solid State Communications 2007;143(1-2):47 – 57. Exploring graphene - Recent research advances.

[49] Foster, C.E., Barham, B.P., Reid, P.J.. Resonance raman intensity analysis of chlorine dioxide dissolved in chloroform: The role of nonpolar solvation. The Journal of Chemical Physics 2001;114(19):8492–8504.